

Spin-phonon coupling in hole-doped pyrochlore iridates $Y_2(\text{Ir}_{1-x}\text{Ru}_x)_2\text{O}_7$: A Raman scattering study

Harish Kumar

School of Physical Sciences, Jawaharlal Nehru University, New Delhi - 110067, India.

V. G. Sathe

UGC-DAE Consortium for Scientific Research, University Campus, Khandwa Road, Indore - 452001, India.

A. K. Pramanik

School of Physical Sciences, Jawaharlal Nehru University, New Delhi - 110067, India.

Abstract

Temperature dependent Raman scattering measurements have been performed to explore unusual coupling between magnetism and crystal structure in doped pyrochlore iridate $Y_2(\text{Ir}_{1-x}\text{Ru}_x)_2\text{O}_7$ with $x = 0.0, 0.05$ and 0.2 . The parent $Y_2\text{Ir}_2\text{O}_7$ shows an onset of magnetic ordering around ~ 160 K (T_N) which monotonically decreases with Ru doping. Further, magnetic moment also decreases with progressive substitution of Ru. Substitution of Ru^{4+} ($4d^4$) for Ir^{4+} ($5d^5$) does not introduce significant modification in structural parameters, however, the magnetic transition temperature decreases systematically with doping. Raman scattering data show an anomalous change in A_{1g} and P_3 Raman mode frequency and line-width across T_N of individual samples. We further show that the shifting of Raman mode frequency with temperature exhibits a strong deviation from anharmonic decay around and below the T_N of respective samples which underlines a spin-phonon coupling in these materials.

1. Introduction

Iridium based pyrochlore materials ($A_2\text{Ir}_2\text{O}_7$, $A =$ rare-earth elements) are of particular interest as they have been predicted to give rise many exotic topological phases.[1, 2] The $5d$ based iridates are unique due to its heavy character and extended d -orbitals. The spin-orbital coupling (SOC) and electronic correlation (U) effect show a comparable energy scale. The interplay between SOC and U is considered to give rise many interesting and novel physical properties. Moreover, pyrochlore materials have in-built frustration which arises from the structural geometry where the A and Ir cations form inter-penetrating corner-shared tetrahedra. This frustration, in general, again induces many other phenomena such as spin glass, spin ice, spin liquid, etc.[3, 4, 5, 6, 7, 8] However, calculation has shown that inclusion of Dzyaloshinskii-Moriya interaction (DMI),

which is very evident in SOC dominant systems, removes the spin degeneracy and favors the long-range ordered (LRO) state at low temperature in otherwise frustrated systems.[9]

The physical properties of pyrochlore iridates have been shown to evolve with A-site element: from magnetic and insulating to complex metallic and nonmagnetic phases with increasing ionic radii of A-ion.[10] This indicates that crystal structure particularly trigonal distortion of IrO_6 octahedra has crucial role in influence the physical properties which is directly related to the x -coordinate of O-atom (X_p -parameter). A recent theoretical study has predicted that this distortion is mainly associated with to F_{2g} phonon modes.[11] Among the pyrochlore iridates, $Y_2\text{Ir}_2\text{O}_7$ is an ideal system because Y^{3+} is nonmagnetic. Therefore, the physical properties are largely governed by Ir sublattice. The $Y_2\text{Ir}_2\text{O}_7$ shows insulating behavior throughout temperature and magnetic ordering around 160 K.[12, 13, 14, 15, 16, 17, 18, 19] The low temperature magnetic state of this material is, however, a debated issue. While

Email address: akpramanik@mail.jnu.ac.in (A. K. Pramanik)

the neutron measurements [12] show no sign of magnetic long-range ordering, previous muon spin relaxation investigations[13] have shown spontaneous oscillations in muon asymmetry below 150 K, indicating a LRO state at low temperature. Theoretically, this material is proposed to be a Weyl-type semimetal (WSM) with a noncoplanar AFM structure.[20] Thus, $Y_2Ir_2O_7$ offers an ideal system to study the interplay between SOC and U with the Ir-site substitution and to study the effect of structure distortion (trigonal) on the related properties.

With an aim to tune the SOC and U parameters as well as to understand the role of structural distortion in $Y_2Ir_2O_7$, we have substituted Ru at Ir-site in $Y_2(Ir_{1-x}Ru_x)_2O_7$. Ru^{4+} ($4d^4$) substitution for Ir^{4+} ($4d^5$) in present series which act for hole doping and simultaneously it will tune both SOC and U , however, in opposite manner. Ru^{4+} ($4d^4$) has comparable ionic radii with Ir^{4+} ($4d^5$), thus no major structural modifications is expected in this series. Ru substitution in $Y_2Ir_2O_7$, previously, have shown the suppression of magnetic ordering and resistivity.[19] Recently, Raman study has shown an interesting correlation between structure and magnetic behavior in Ir-based other compounds, such as, Sr_2IrO_4 and Na_2IrO_3 . [21, 22, 23] There is exists Raman scattering studies on pyrochlore iridates,[24, 25] however, a direct correlation between magnetic and structure parameters is not established yet. Given that pyrochlore structure has complex structural organization and the Ir-based materials have reasonable SOC, which is weakened with Ru in present series, this present effort to investigate the magneto-structural coupling with Raman scattering measurements and the role of SOC would provide vital information in this class of materials.

In this paper, we present the results of magnetic and Raman scattering measurements for $Y_2(Ir_{1-x}Ru_x)_2O_7$ series with composition $x = 0.0, 0.05$ and 0.2 . Magnetic susceptibility data show that both the magnetic moment at low temperature and the magnetic irreversibility temperature (T_N) decrease with Ru substitution. With Ru doping, the overall system retains the original structural symmetry, however, the lattice parameters show an evolution with Ru content. Ru substitution reduces the trigonal distortion of IrO_6 octahedra in this series. Temperature dependent Raman scattering measurements for $Y_2(Ir_{1-x}Ru_x)_2O_7$ series show anomalous change in frequency and line width of Raman A_{1g} and P_3 mode around magnetic ordering temperature (T_N) which suggest the presence of spin-phonon coupling.

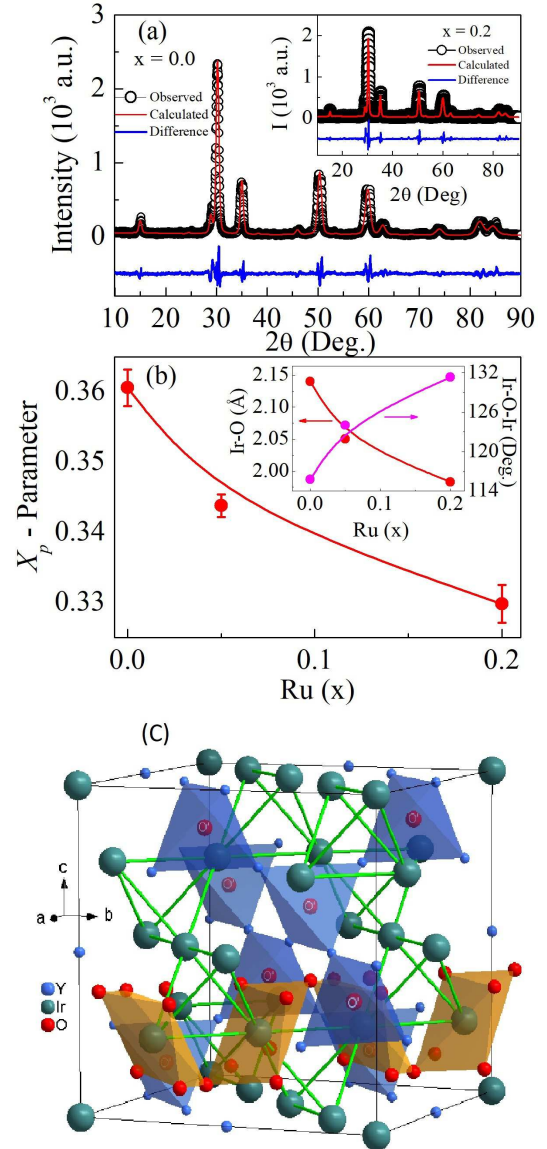


Figure 1: (a) XRD pattern of $Y_2(Ir_{1-x}Ru_x)_2O_7$ ($x = 0.0$) collected at room temperature along with Rietveld refinement. Inset shows XRD pattern along with Rietveld refinement for $x = 0.2$ composition. (b) X_p -parameter of O-atom is shown as a function of Ru doping for $Y_2(Ir_{1-x}Ru_x)_2O_7$ series. Inset shows Ir-O bond length and Ir-O-Ir bond angle as a function of Ru (x). (c) Cubic pyrochlore structure showing the Y_4O' tetrahedra (Blue), $Ir_4\Diamond$ tetrahedra (Green) and IrO_6 octahedra (light orange)

2. Experimental Details

Series of polycrystalline materials $Y_2(Ir_{1-x}Ru_x)_2O_7$ ($x = 0.0, 0.05$, and 0.2) have been prepared using conventional solid state method. Details of sample preparation and characterization are given in Ref.[18, 19]. The

phase purity of the samples have been checked using powder x-ray diffraction (XRD) using a Rigaku made diffractometer with $\text{CuK}\alpha$ radiation. The XRD data have been collected in the 2θ range of $10 - 90^\circ$ at a step of $\Delta 2\theta = 0.02^\circ$. The data have been refined using Reitveld refinement program (FULLPROF) for structural analysis by Young *et al.*[26] DC Magnetization (M) measurements have been carried out with a vibrating sample magnetometer (PPMS, Quantum Design). Temperature dependent Raman spectra have been collected using Diode based laser ($\lambda = 473 \text{ nm}$) coupled with a Labram-HR800 micro-Raman spectrometer. It is a single spectrometer with 1800 groves/mm grating and a peltier cooled CCD detector with a overall spectral resolution of $\sim 1 \text{ cm}^{-1}$. For the low temperature Raman measurements, the material has been mounted on a THMS600 stage from Linkam UK, with temperature stability of $\pm 0.1 \text{ K}$.

3. Results and Discussions

3.1. Structural analysis

Fig. 1 (a) shows the room temperature pattern of XRD data along with Rietveld analysis for the parent compound $\text{Y}_2\text{Ir}_2\text{O}_7$ ($x = 0.0$). The XRD data for parent material match well with previous studies.[12, 13, 17, 18] The Rietveld refinement show the sample is in single phase and crystallizes in cubic $Fd\bar{3}m$ phase (Fig. 1 (a)) with lattice constant $a = 10.244(1) \text{ \AA}$. The inset of Fig. 1 (a) shows the Rietveld refinement of XRD data for last sample of the present series i.e., $x = 0.2$. It is clear in inset of Fig. 1 (a) that XRD pattern of $x = 0.2$ does not exhibit any change with Ru content in terms of peak position or impurity peak which implies Ru doping does not cause any major changes in crystal symmetry. This behavior is also expected for Ru doping because of their matching ionic radii ($\text{Ru}^{4+} = 0.62 \text{ \AA}$ and $\text{Ir}^{4+} = 0.625 \text{ \AA}$). However, the Rietveld analysis of XRD data for all samples shows that structural parameters (X_p -parameter, bond-length and bond-angle) evolve continuously with Ru doping in the present series as shown in Fig. 1 (b). Fig. 1 (c) depicts unit cell atomic arrangement of cubic- $Fd\bar{3}m$ pyrochlore structure for the parent compound $\text{Y}_2\text{Ir}_2\text{O}_7$ showing it has interpenetrating two types of sub-lattices of tetrahedra, i.e., $\text{Y}_4\text{O}'$ and Ir_4O , where O implies empty center-site (8a site). As Y^{3+} is nonmagnetic in parent case so the tetrahedra of Ir cations only introduces magnetic interaction/frustration in $\text{Y}_2\text{Ir}_2\text{O}_7$.

Pyrochlore materials, generally, adopt the cubic crystallographic phase with $Fd\bar{3}m$ space group.[27] There

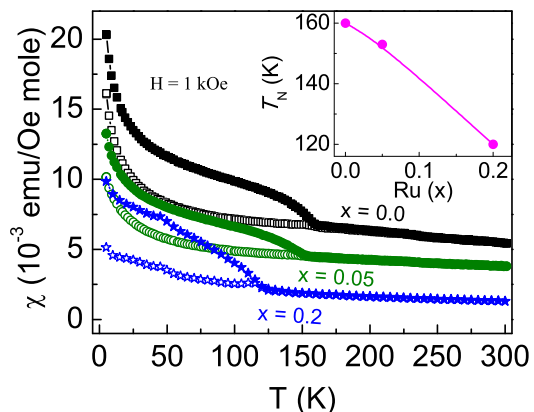


Figure 2: Temperature dependent magnetic susceptibility data measured in 1 kOe field under ZFC and FC protocol are shown for $\text{Y}_2(\text{Ir}_{1-x}\text{Ru}_x)_2\text{O}_7$ series. Inset shows variation of transition temperature T_N with Ru substitution for the same series.

are two free structural parameters in pyrochlore structure such as, lattice constant (a) and x -coordinate of oxygen $48f$ -site (X_p -parameter). Apart from the lattice parameters, X_p -position of the oxygen is directly related to the structural organization of IrO_6 octahedra in the pyrochlore structure. In general, the six oxygen ions are coordinated around Ir^{4+} cation to form a distorted IrO_6 octahedra. The amount of (trigonal) distortion of the IrO_6 octahedra can be determined from the information of the X_p -parameter of oxygen atom. In IrO_6 octahedra, each oxygen ion is at equal distance from central Ir ion. For $x_{ideal} = 0.3125$, Ir^{4+} cations form an ideal IrO_6 octahedra and if $x = 0.375$, the IrO_6 octahedra are distorted where A cations form a perfect cube. The pyrochlore structure consists of two types inter-penetrating layer of tetrahedra i.e., $\text{Y}_4\text{O}'$ and Ir_4O , where O implies empty center-site (8a site) as illustrated in Fig. 1 (c). All pyrochlore iridates usually have larger X_p -value than this ideal value, indicating trigonal distortion to the octahedra which lowers the cubic symmetry and gives trigonal crystal field.[11, 28, 29]

The variation in X_p -parameter of oxygen atom with Ru is shown in Fig. 1 (b). The X_p -value for the parent system is found around 0.36 which is large compared to the ideal value ($x_{ideal} = 0.3125$) and suggests the IrO_6 octahedra's are distorted and compressed. As evident in figure, the X_p -value has decreased with progressive substitution of Ru content. The decrease of the X_p -value in Fig. 1 (b) suggests that the system is leading towards perfect octahedra, hence trigonal crystal field is reduced. As the oxygen atoms occupying the $48f$ -site form the IrO_6 octahedra, hence, the $\langle \text{Ir-O-Ir} \rangle$ bond-angle and Ir-O bond-length are related to

the X_p -parameter and plays an important role in determining the physical properties. The evolution of Ir-O bond-length and $\langle \text{Ir-O-Ir} \rangle$ bond-angle for the present series are shown inset of Fig. 1 (b). It is evident in figure that the bond-length decreases while bond-angle simultaneously increases with progressive substitution of Ru. This variation of Ir-O bond-length and angle suggests that distortion in IrO_6 octahedra is reduced and increases Ir(5d)/Ru(4d) and O(2p) orbital overlapping which facilitates the hopping of the Ir electrons.

3.2. Magnetization Study

Fig. 2 shows the temperature dependent magnetic susceptibility (χ) data for $\text{Y}_2(\text{Ir}_{1-x}\text{Ru}_x)_2\text{O}_7$ series, where the data have been collected under zero-field cooled (ZFC) and field-cooled (FC) protocol in an applied field of 1 kOe. In Fig. 2, it is quite obvious that $\chi(T)$ data for parent material ($x = 0.0$) shows a magnetic irreversibility around $T_N = 160$ K which marks an antiferromagnetic type magnetic phase transition where below this temperature a large bifurcation between the χ_{ZFC} and χ_{FC} branches is observed. On further cooling, we find that below around 50 K the magnetization increases very sharply. As evident in Fig. 2, with Ru substitution the notable observations are, i) the low temperature magnetic moment decreases, ii) difference between χ_{FC} and χ_{ZFC} decreases and iii) the bifurcation temperature (T_N) shift toward low temperature. The composition dependent T_N is shown in inset of Fig. 2. Moreover, the decrease of T_N is almost linear with Ru substitution and we find that magnetic irreversibility temperature $T_N \sim 120$ K for 20% doping of Ru ($x = 0.2$) which is quite consistent with previous study.[19]

It can be further observed in Fig. 2 that the magnetic susceptibility decreases with increasing x which is rather surprising as data suggest substitution of Ru^{4+} ($S = 1$) for Ir^{4+} ($J_{eff} = 1/2$) causes weakening and suppression of magnetic transition in $\text{Y}_2(\text{Ir}_{1-x}\text{Ru}_x)_2\text{O}_7$. Generally, the pyrochlore lattice with Heisenberg-type nearest neighbor interactions show collinear type antiferromagnetic (AFM) spin structure where frustration is a very inherent feature. An additional Dzyaloshinskii-Moriya (DM) interaction, which mainly originates from the spin-orbit coupling (SOC), results in non-collinear type magnetic structures.[9] In present case, the introduction of Ru in place of Ir is expected to reduce the SOC effect, hence it would derive toward the system with more collinear type AFM spin ordering. This can lead to decrease of moment. Moreover, recent theoretical calculations have shown that with increasing U the magnetic state in $\text{Y}_2\text{Ir}_2\text{O}_7$ moves from non-collinear AIAO state to AFM spin structure.[30, 31] Therefore,

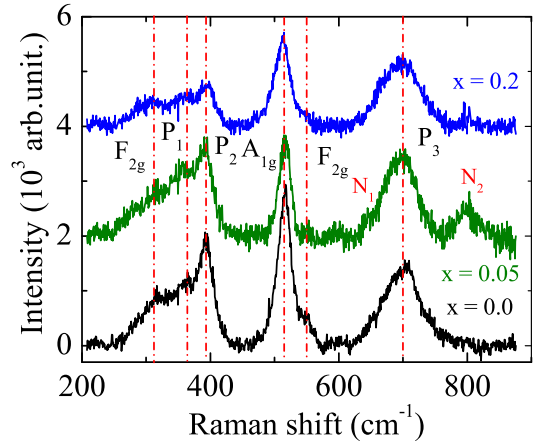


Figure 3: Raman spectra measured at room temperature are shown for $\text{Y}_2(\text{Ir}_{1-x}\text{Ru}_x)_2\text{O}_7$ ($x = 0.0, 0.05$ and 0.2). Raman data for $x = 0.05$ and 0.2 are shifted vertically for clarity.

the decrease in magnetic moment may be due to the tuning of SOC and U with Ru doping. In Fig. 2, therefore, magnetic susceptibility data in comparison to $x = 0.1$ the data for $x = 0.2$ look significantly reduced. Here, it can be further mentioned that the other end member of this present series, i.e., $\text{Y}_2\text{Ru}_2\text{O}_7$ ($x = 1.0$) shows an antiferromagnetic transition ($T_N \sim 76$ K) and large bifurcation between ZFC and FC magnetization at low temperature.[32] Additionally, this materials also shows reasonably large frustration which suggests Y based pyrochlore materials have inherent frustration.

3.3. Temperature dependence Raman study for $\text{Y}_2\text{Ir}_2\text{O}_7$

To understand further the structural evolution, Raman spectroscopy has been carried out which are primarily sensitive to metal ion-oxygen bond vibrations as well as to local structural disorder. Fig. 3 shows Raman spectra for the $\text{Y}_2(\text{Ir}_{1-x}\text{Ru}_x)_2\text{O}_7$ series with composition $x = 0.0, 0.05$ and 0.2 at room temperature. According to previous structural discussions, $\text{Y}_2\text{Ir}_2\text{O}_7$ belongs to the cubic space group of $Fd\bar{3}m$. For this space group, six Raman active modes are expected according to the factor group analysis, $\Gamma^R = A_{1g} + E_g + 4F_{2g}$ which are mainly involved in motion of oxygen atoms.[24, 25] At room temperature, we have observed six Raman peaks at 314, 361, 393, 516, 552, and 700 cm^{-1} which are assigned to $F_{2g}, P_1, P_2, A_{1g}, F_{2g}$ and P_3 Raman modes, respectively. The observed modes for $\text{Y}_2\text{Ir}_2\text{O}_7$ are fully consistent with the previous reported studies of the pyrochlore iridates.[24, 25] Out of all, the A_{1g} mode (515 cm^{-1}) has particular importance in the pyrochlore structure because it is directly involved in

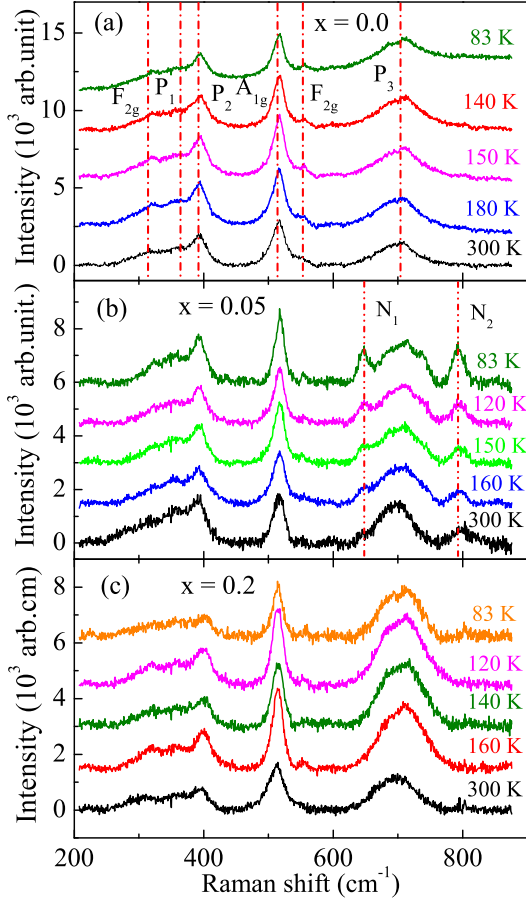


Figure 4: Raman spectra have been shown for $x = 0.0$ (a), $x = 0.05$ (b) and $x = 0.2$ (c) for $Y_2(Ir_{1-x}Ru_x)_2O_7$ series at selected temperatures.

the trigonal distortion of IrO_6 octahedra through modification of $\langle Ir-O-Ir \rangle$ bond angle.[33] Therefore, A_{1g} mode is involved in the modulation of oxygen position coordinate (X_p) where the vibration of oxygen atoms at $48f$ site plays a major role.[34, 35] Similarly, F_{2g} mode is assigned to the mixture of A-O and Ir-O bond stretching vibrations and E_g mode corresponds to IrO_6 bending vibrations.[36] Therefore, both A_{1g} and E_g modes are basically considered as bending mode and largely influenced by changes with $\langle Ir-O-Ir \rangle$ bond angle.

The P_3 phonon mode in pyrochlore materials, on the other hand, is another vital parameter which is mostly observed around 700 cm^{-1} and is related to Ir-O bond stretching which has significant influence on the $Ir(5d)-O(2p)$ hybridization.[37, 38] With Ru substitution, all the six modes are observed in doped samples. In addition, $x = 0.05$ material shows two extra peaks at 648 , and 792 cm^{-1} which are marked as N_1 and N_2 modes, respectively. The N_2 mode is also observed for $x =$

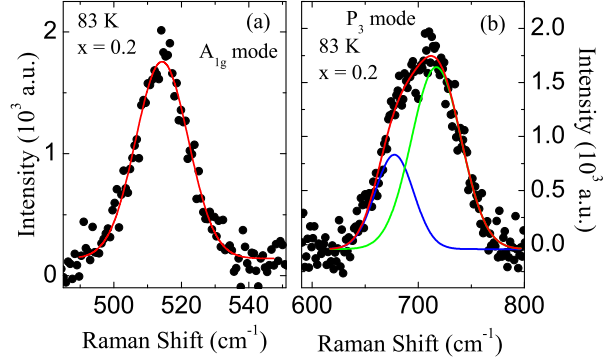


Figure 5: (a) and (b) show lineshape of A_{1g} and P_3 phonon modes at temperature 83 K for $x = 0.2$ sample, respectively. The solid red line in figure for A_{1g} and P_3 modes is due to single and multiple peak fitting.

0.2 but intensity of N_2 mode for $x = 0.2$ is very low. The observed new modes are commonly found in the frequency range from 600 to 900 cm^{-1} in pyrochlores [34, 35] and are often assigned as the second order Raman scattering.[25, 39] In order to understand an evolution of structural symmetry with temperature in the parent and doped materials, we have performed the temperature dependent Raman measurements. Fig. 4 (a) shows the representative Raman spectrum of $Y_2Ir_2O_7$ at 300 , 180 , 150 , 140 and 83 K where the temperatures correspond to the room temperature paramagnetic state (300 K), just above (180 K) and below (140 K) the magnetic transition temperature T_N (160) and low-temperature state (83 K). It is evident in the figure that there is no noticeable changes in Raman active modes in terms of shifting of peak position or appearance of new peak with lowering the temperature. This implies that there is no visible change in structural symmetry with temperature which agrees well with the temperature dependence of XRD and neutron scattering measurements.[18, 12]

As seen in Fig. 1 (b), all structural lattice parameters show an evolution with doping content (x). Therefore, we now turn to the temperature dependent Raman study for the doped samples. Figs. 4 (b) and (c) show temperature dependent Raman spectrum for the doped $x = 0.05$ and 0.2 samples, respectively. With lowering the temperature, no changes in low frequency modes are observed for 5% doped sample but the A_{1g} (515 cm^{-1}) and the new N_1 and N_2 modes become more sharp and intense. For 20% doped compound, the intensity of A_{1g} mode increases with decreasing temperature. To understand further the role of phonon parameters with temperature, we have performed detail analysis of temperature dependent Raman data for all the samples.

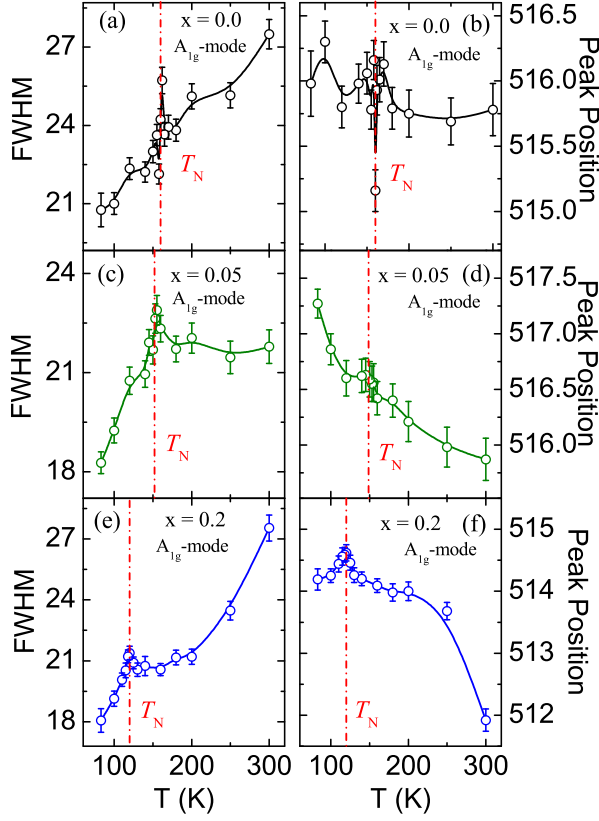


Figure 6: (a), (c), (e) show full width at half maximum (FWHM), and (b), (d), (f) show position/frequency of the A_{1g} phonon mode as a function of temperature for $x = 0.0, 0.05$ and 0.2 samples at upper, middle and lower panel, respectively.

The A_{1g} (515 cm^{-1}) and P_3 (700 cm^{-1}) mode play an important role in pyrochlore structure. We have performed detail analysis of these two modes in order to understand the their evolution with doping as well as with temperature, particularly around the magnetic transition temperature (T_N). As evident in Fig. 4 that the A_{1g} peaks are single and sharp while the P_3 peaks are broad and consist of multiple peaks. Therefore, we have performed single and multiple peak fitting for A_{1g} and P_3 modes, respectively. The representative peak fitting for these A_{1g} and P_3 modes is shown in Figs. 5a and 5b, respectively for $x = 0.2$ sample at 83 K. The evolution of line-width as represented by full width at half maximum (FWHM) and position of A_{1g} phonon mode with temperature are shown for the parent material $x = 0.0$ as shown in Fig. 6 (a) and (b), respectively. With lowering the temperature, frequency/position of A_{1g} phonon mode show fluctuations. This mode is directly associated with the oxygen X_p -parameter of IrO_6 octahedra therefore, the observed fluctuations with tempera-

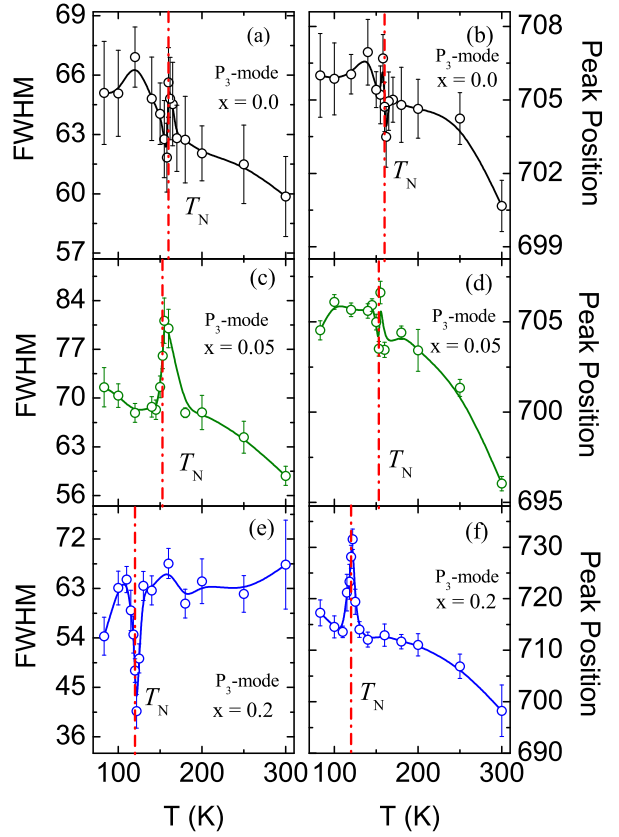


Figure 7: (a), (c), (e) show full width at half maximum (FWHM), and (b), (d), (f) show position/frequency of the P_3 phonon mode as a function of temperature for $x = 0.0, 0.05$ and 0.2 samples at upper, middle and lower panel, respectively.

ture in the frequency of A_{1g} mode are in good agreement with the previously reported temperature dependent of X_p -parameter obtained from XRD analysis.[18] The change in line-width is about -24.5% over the temperature range. It is important to note that a discernible anomaly in FWHM of A_{1g} phonon mode is observed around T_N . This anomaly in Raman data may arise due to sudden rotation/distortion of IrO_6 octahedra across T_N temperature (160 K).

For Ru doped materials, Figs. 6 (c) and (d) depict the FWHM and the frequency of the 515 cm^{-1} A_{1g} -mode as function of temperature for $x = 0.05$ sample. Fig. 6 (c) shows the FWHM of the A_{1g} mode decreases with the lowering temperature where the change in FWHM is $\sim -16.2\%$ over this temperature regime. It is important to note that FWHM of A_{1g} mode show a clear anomaly around 152 K which is corresponds to the magnetic ordering temperature T_N of $x = 0.05$ material. The change in A_{1g} mode position with temperature is presented in

Fig. 6 (d) for $x = 0.05$ which increases with decreasing the temperature and shows a distinct anomaly around T_N (~ 152 K). This change in position of A_{1g} mode is not substantial, as we calculate the change is about 0.16% over this temperature region. Compared to parent material ($x = 0.0$), the peaks in both FWHM and position of A_{1g} mode is shifted by 8 K for $x = 0.05$ which is consistent with a suppression of the magnetic ordering as presented in Fig. 2.

With further increasing the doping concentration to $x = 0.2$, Fig. 6 (e) shows the FWHM of the A_{1g} mode which decreases with decreasing temperature where the change in FWHM is $\sim 34.4\%$ over this temperature regime. Moreover, for the $x = 0.2$, Fig. 6 (f) shows the temperature evolution of the position of A_{1g} mode which increases with decreasing the temperature. We calculate the change in position of A_{1g} is about 0.4% (~ 2 cm^{-1}) over whole temperature region. We further observe a change in phonon frequency of A_{1g} modes around 4 cm^{-1} for $x = 0.2$ sample at room temperature compared to parent material. The position of A_{1g} mode also shows a distinct anomalies around ~ 120 K which is corresponding to magnetic ordering temperature (T_N) of $x = 0.2$. The observed anomalies in the FWHM and the position of A_{1g} mode around T_N for both the doped material ($x = 0.05, 0.2$) is in good agreement with suppression of the magnetic ordering with Ru content (x). The previous Raman study for the other iridate systems $\text{Sr}_2(\text{Ir}_{1-x}\text{Ru}_x)\text{O}_4$ reveals similar evolution of phonon parameters around the magnetic ordering temperature.[21, 22] The observed anomaly in Raman data for the present series may arises due to sudden rotation/distortion of IrO_6 octahedra across T_N .

We have earlier discussed the importance of the P_3 phonon mode which is observed around 700 cm^{-1} . Here, we have analyzed the temperature dependent Raman data in order to understand the evolution of the P_3 -phonon mode across magnetic ordering temperature in the present series. Fig 7 (a), (c), (e) and (b), (d), (f) show the evolution of FWHM and frequency/position of P_3 -phonon mode with temperature for the present $\text{Y}_2(\text{Ir}_{1-x}\text{Ru}_x)_2\text{O}_7$ series, respectively. We find that the FWHM of P_3 phonon mode for $x = 0.0$ and 0.05 increases with decreasing the temperature and shows a distinct anomaly around T_N . While, the change in FWHM of P_3 phonon mode for $x = 0.2$ is small but it exhibits a downfall anomaly around T_N . The position of P_3 phonon mode for $x = 0.0, 0.05$ and 0.2 mostly increases with decreasing the temperature in contrast to A_{1g} mode. The observed phonon anomalies in terms of peak position and FWHM of P_3 mode around T_N for all the materials is in good agreement with suppression of

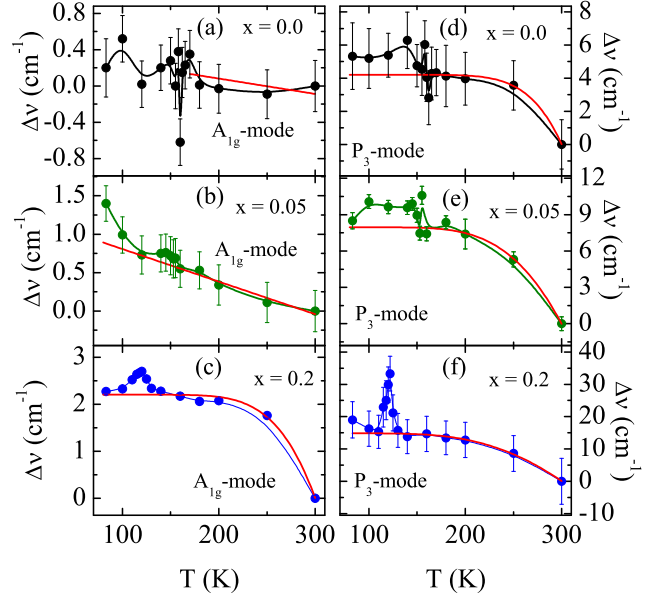


Figure 8: (a), (c), (e) show temperature evolution of the A_{1g} phonon frequency shift and (b), (d), (f) for the P_3 phonon frequency shift for $x = 0.0, 0.05$ and 0.2 samples at upper, middle and lower panel, respectively. Solid lines are fit corresponding to anharmonicity predictions (Eq. 1).

the magnetic ordering temperature T_N with Ru content (x).

With material composition (x), the phonon frequency of P_3 mode also modifies. For $x = 0.2$, we find the change in phonon frequency of P_3 about 3 and 22 cm^{-1} at room temperature and magnetic transition temperature, respectively compared to $x = 0$ material. Given that this change of phonon frequency represents a modification of electronic and local structures, these results imply that the Ru has nonuniform effect on shifting of phonon frequency for A_{1g} and P_3 modes. Nonetheless, these changes are comparable with other iridate samples. For instance, in case of $\text{Sr}_2\text{Ir}_{1-x}\text{Ru}_x\text{O}_4$ the change is around 8 cm^{-1} for $x = 0.2$ sample.[22]

Above discussions imply that the anomalous changes in position and in line-width (FWHM) of the Raman mode frequency around the magnetic ordering temperature mainly occur due to spin-phonon coupling in these systems. To understand further the presence of spin-phonon coupling in present series, we have analyzed the Raman data of present series with the following anharmonic decay model[40]

$$\omega(T) = \omega_0 - C \left[1 + \frac{2}{\left[\exp\left(\frac{\hbar\omega_0}{2k_B T}\right) - 1 \right]} \right] \quad (1)$$

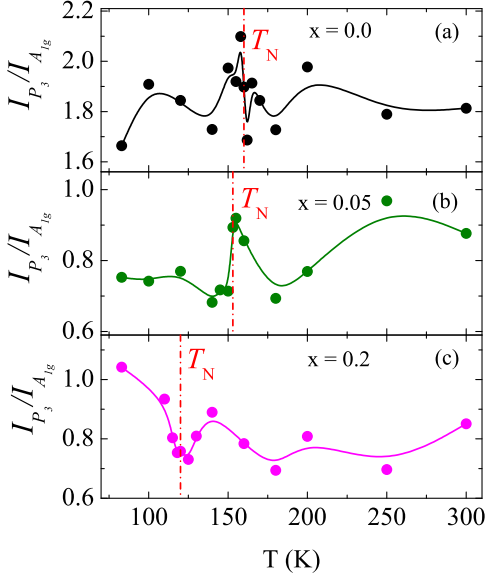


Figure 9: (a), (b) and (c) show temperature dependence of the relative intensity of the A_{1g} to the P_3 phonon mode for $x = 0.0, 0.05$ and 0.2 samples, respectively.

where ω_0 and C are the intrinsic frequency of the optical mode and anharmonic coefficient, respectively. The term $[\exp(\frac{\hbar\omega_0}{2k_B T}) - 1]^{-1}$ corresponds to the thermal population factor of the acoustic modes. In general, temperature dependent change of phonon mode frequency is observed to follow anharmonic two-channel-phonon decay which is given in Eq. 1 (assuming negligible contribution from lattice expansion/contraction and/or electron-phonon coupling term). However, due to presence of prominent spin-phonon coupling which is caused by change in exchange interaction by lattice vibration, the phonon mode frequency shift shows a deviation from anharmonic decay around the magnetic phase transition. Granado *et al*[41] has proposed a model for spin-phonon coupling showing the contribution can be expressed as,

$$\omega_{s-ph}(T) = \lambda \langle S_i \cdot S_j \rangle \quad (2)$$

where λ is spin-phonon coupling constant and $\langle S_i \cdot S_j \rangle$ is spin correlation function. At low temperatures and particularly near to the magnetic phase transition, the spin-spin correlation develops, hence its contribution become prominent showing a marked deviation from Eq. 1. As spin-spin exchange interaction is key to spin-phonon coupling, spin-orbit coupling which is prominent in Ir-based samples also plays a vital role in exchange coupling.

We have shown the shifting of phonon mode frequency $\Delta\nu$ (normalized to room temperature) for A_{1g} and P_3 modes in Fig. 8 (a), (b), (c) and (d), (e), (f), respectively for $Y_2(\text{Ir}_{1-x}\text{Ru}_x)_2\text{O}_7$ series. The solid lines in Fig. 8 are due to fitting with Eq. 1. It is clear in figure that for parent compound ($x = 0.0$), the frequency shifting ($\Delta\nu$) can be roughly fitted in high temperature region but below and around $T_N = 160$ K, the $\Delta\nu$ shows fluctuations similar to the position of A_{1g} mode (Fig. 6 (b)). We have discussed before that the A_{1g} phonon mode corresponds to trigonal distortion of IrO_6 octahedra through the vibration of O-atom. Therefore, this mode is directly related to the oxygen X_p -parameter of IrO_6 octahedra. The observed fluctuations with temperature in the A_{1g} phonons are in good agreement with the previously reported temperature dependent X_p -parameter obtained from XRD analysis.[18] However, with increasing Ru concentration, the high temperature frequency shift ($\Delta\nu$) can be fitted well with Eq. 1. It is noticeable in figure that $\Delta\nu$ strongly deviates from fitting of Eq. 1 across the magnetic ordering temperature (T_N).

In case of P_3 mode, the $\Delta\nu$ shows a large deviation from Eq. 1 across T_N in parent compound. This deviation from Eq. 1 in Fig. 8 (d) underlines the fact that this has prominent spin-phonon coupling. With Ru substitution, the $\Delta\nu$ deviation for P_3 mode shows a pronounced softening across T_N of respective samples (Figs. 8e and 8f). It is interesting that deviation of P_3 mode reduces with Ru substitution while through Ru^{4+} contributes to magnetic ordering. We speculate that the tuning of SOC with Ru doping modifies the spin-spin interaction which may lead to softening of $\Delta\nu$ deviation across T_N in higher doped samples. It is well known fact that SOC induce distortion of IrO_6 octahedra induces Dzyaloshinskii-Moriya (DM) type asymmetric interaction which subsequently results in a weak ferromagnetic behavior in Ir-based Sr_2IrO_4 . [42, 43] This material otherwise exhibits Heisenberg-type antiferromagnetic exchange interaction with magnetic transition temperature ~ 240 K.[43] In fact, we observe a huge change in Ir-O-Ir bond angle from around 115 to 131° with 20% of Ru doping while both Ir^{4+} and Ru^{4+} have matching ionic radii (see Fig. 1(b)). Therefore, softening of deviation in frequency shifting of P_3 mode in Fig. 8 is likely to be associated with tuning of SOC in $Y_2(\text{Ir}_{1-x}\text{Ru}_x)_2\text{O}_7$ series.

We have further looked at the ratio of A_{1g} and P_3 phonon modes in present series which are related to Ir-O bond angle and bond length, respectively (discussed above). We have plotted the ratio of P_3 and A_{1g} phonon intensity mode as a function of temperature for $x = 0.0, 0.05$ and 0.2 in Fig. 9. For parent material ($x = 0.0$),

with decreasing the temperature the $I_{P_3}/I_{A_{1g}}$ shows similar type of fluctuations as observed for position of A_{1g} phonon mode (Fig. 6 (b) and Fig. 8 (a)). The intensity ratio of $I_{P_3}/I_{A_{1g}}$ for $x = 0.05$ shows a small variation with temperature, however, it shows an anomalous change around the magnetic ordering temperature (T_N). For the highest doped material i.e., $x = 0.2$, the intensity ratio of $I_{P_3}/I_{A_{1g}}$ shows a distinct anomaly around T_N . Further, we have separately analyzed the temperature dependent intensity data of A_{1g} and P_3 mode for $x = 0.2$ (not shown). While both A_{1g} and P_3 modes show an anomalous change around T_N but the change in A_{1g} mode is comparatively high.

Our Results show that Ru substitution in $Y_2(\text{Ir}_{1-x}\text{Ru}_x)_2\text{O}_7$ series has prominent effects on structural behavior where the system retains its original structural symmetry but the phonon modes show an evolution with temperature. The anomalous changes in frequency and line-width of the Raman modes around the magnetic ordering temperature are quite interesting. Further, the anomaly in $I_{P_3}/I_{A_{1g}}$ ratio and deviation in frequency shifting from anharmonic decay across T_N for both I_{P_3} and $I_{A_{1g}}$ modes (Fig. 9) suggest a reasonable spin-phonon coupling in present $Y_2(\text{Ir}_{1-x}\text{Ru}_x)_2\text{O}_7$. These results in present study will certainly be helpful to understand the low temperature nature of structural behavior with the magnetic behavior in pyrochlore iridates.

4. Conclusion

To summarize, we have presented Raman scattering study on series of polycrystalline samples $Y_2(\text{Ir}_{1-x}\text{Ru}_x)_2\text{O}_7$ ($x = 0.0, 0.05$ and 0.2). With substitution of Ru, system retains its original crystal structure symmetry, however, structural parameters evolve with the Ru doping (x). Magnetic susceptibility data reveal both the onset of magnetic irreversibility and the magnetic moment decreases with Ru doping. Temperature dependent Raman data of parent material $Y_2\text{Ir}_2\text{O}_7$ does not exhibits any structural change around magnetic transition T_N , but Raman mode frequency and line-width show an anomalous change around the magnetic transition temperature T_N . With Ru substitution, the frequency and line-width of A_{1g} and P_3 phonon mode also exhibit an anomaly around T_N of respective samples. Shifting of Raman mode frequency with temperature shows a deviation from anharmonic decay model around respective magnetic ordering temperature which signifies prominent spin-phonon coupling in these samples. Tuning of SOC with Ru substitution is also ev-

ident in softening of frequency deviation from anharmonic decay.

5. Acknowledgment

We acknowledge UGC-DAE CSR, Indore for the magnetization and Raman spectroscopy measurements. We are thankful to Dr. Alok Banerjee for the magnetization measurements and discussions. We are thankful to Mr. Kranti Kumar and Ajay Kumar Rathore for the helps in measurements. HK acknowledges UGC, India for BSR fellowship.

References

- [1] D. Pesin and L. Balents, *Nature Phys* **6**, 376 (2010).
- [2] W. Witczak-Krempa, G. Chen, Y. B. Kim, and L. Balents, *Annual Rev. of Condens. Matter Physics*. **5**, 57 (2014).
- [3] M. J. P. Gingras, C. V. Stager, N. P. Raju, B. D. Gaulin, and J. E. Greedan, *Phys. Rev. Lett.* **78**, 947 (1997).
- [4] S. Yoshii and M. Sato, *J. Phys. Soc. Jpn.* **68**, 3034 (1999).
- [5] J. S. Gardner, S. R. Dunsiger, B. D. Gaulin, M. J. P. Gingras, J. E. Greedan, R. F. Kiefl, M. D. Lumsden, W. A. MacFarlane, N. P. Raju, J. E. Sonier, I. Swainson, and Z. Tun, *Phys. Rev. Lett.* **82**, 1012 (1999).
- [6] S. Nakatsuji, Y. Machida, Y. Maeno, T. Tayama, T. Sakakibara, J. van Duijn, L. Balicas, J. N. Millican, R. T. Macaluso and J. Y. Chan, *Phys. Rev. Lett.* **96**, 087204 (2006).
- [7] S. T. Bramwell, M. J. Harris, B. C. den Hertog, M. J. P. Gingras, J. S. Gardner, D. F. McMorrow, A. R. Wildes, A. L. Cornelius, J. D. M. Champion, R. G. Melko, and T. Fennell, *Phys. Rev. Lett.* **87**, 047205 (2001).
- [8] H. Fukazawa, R. G. Melko, R. Higashinaka, Y. Maeno, and M. J. P. Gingras, *Phys. Rev. B* **65**, 054410 (2002).
- [9] M. Elhajal, B. Canals, R. Sunyer and C. Lacroix, *Phys. Rev. B* **71**, 094420 (2005).
- [10] K. Matsuhira, M. Wakeshima, Y. Hinatsu, and S. Takagi, *J. Phys. Soc. Jpn.* **80**, 094701 (2011).
- [11] B.-J. Yang and Y. B. Kim, *Phys. Rev. B* **82**, 085111 (2010).
- [12] M. C. Shapiro, S. C. Riggs, M. B. Stone, C. R. de la Cruz, S. Chi, A. A. Podlesnyak and I. R. Fisher, *Phys. Rev. B* **85**, 214434 (2012).
- [13] S. M. Disseler, C. Dhital, A. Amato, S. R. Giblin, C. de la Cruz, S. D. Wilson, and M. J. Graf, *Phys. Rev. B* **86**, 014428 (2012).
- [14] N. Taira, M. Wakeshima and Y. Hinatsu, *J. Phys.: Condens. Matter* **13**, 5527 (2001).
- [15] H. Fukazawa and Y. Maeno, *J. Phys. Soc. Jpn.* **71**, 2578 (2002).
- [16] M. Soda, N. Aito, Y. Kurahashi, Y. Kobayashi, and M. Sato, *Physica B* **1071**, 329 (2003).
- [17] W. K. Zhu, M. Wang, B. Seradjeh, F. Yang, and S. X. Zhang, *Phys. Rev. B* **90**, 054419 (2014).
- [18] H. Kumar and A. K. Pramanik, *J. Magn. Magn. Mater* **409** 20 (2016).
- [19] H. Kumar, R. S. Dhaka and A. K. Pramanik, *Phys. Rev. B* **95**, 054415 (2017).
- [20] X. Wan, A. M. Turner, A. Vishwanath, and S. Y. Savrasov, *Phys. Rev. B* **83**, 205101 (2011).
- [21] M. F. Cetin, P. Lemmens, V. Gnezdilov, D. Wulferding, D. Menzel, T. Takayama, K. Ohashi, and H. Takagi, *Phys. Rev. B* **85**, 195148 (2012).

- [22] A. Glamazda, W. J. Lee, P. Lemmens, H. Y. Choi, N. Lee, Y. J. Choi and K. Y. Choi, Phys. Rev. B **89**, 104406 (2014).
- [23] S. N. Gupta, P. V. Sriluckshmy, K. Mehlawat, A. Balodhi, D. K. Mishra, S. R. Hassan, T. V. Ramakrishnan, D. V. S. Muthu, Y. Singh and A. K. Sood, Eur. Phys. letter **114**, 47004, (2016)
- [24] H. Han, L. Zhang, H. Liu, L. Ling, W. Tong, Y. Zou, M. Ge, J. Fan, C. Zhang, L. Pi and Y. Zhang, Philosophical Magazine **95**, 3014 (2015).
- [25] T. Hasegawa, N. Ogita, K. Matsuhira, S. Takagi, M. Wakeshima, Y. Hinatsu and M. Udagawa, J. Phys.: Conf. Ser. **200** 012054 (2010).
- [26] R. A. Young, A. Sakthivel, T. S. Moss and C. O. Paiva-Santos, *Users guide to program DBWS-9411*, Atlanta: Georgia Institute of Technology (1994).
- [27] M. A. Subramanian, G. Aravamudan and G. V. Subba Rao, Prog. Solid State Chem. **15**, 55 (1983).
- [28] J. P. Clancy, H. Gretarsson, E. K. H. Lee, Di Tian, J. Kim, M. H. Upton, D. Casa, T. Gog, Z. Islam, Byung-Gu Jeon, Kee Hoon Kim, S. Desgreniers, Yong Baek Kim, S. J. Julian, and Young-June Kim, Phys. Rev. B **94**, 024408, (2016).
- [29] L. Hozoi, H. Gretarsson, J. P. Clancy, B.-G. Jeon, B. Lee, K. H. Kim, V. Yushankhai, P. Fulde, D. Casa, T. Gog, J. Kim, A. H. Said, M. H. Upton, Young-June Kim, and J. van den Brink, Phys. Rev. B **89**, 115111, (2014).
- [30] H. Shinaoka, S. Hoshino, M. Troyer, and P. Werner, Phys. Rev. Lett. **115** 156401 (2015).
- [31] F. Ishii, Y. P. Mizuta, T. Kato, T. Ozaki, H. Weng, and S. Onoda, J. Phys. Soc. Jpn. **84**, 073703 (2015).
- [32] R. Kmieć, Z. Świątkowska, J. Gurgul, M. Rams, A. Zarzycki, and K. Tomala, Phys. Rev. B **74**, 104425 (2006).
- [33] K. Taniguchi, T. Katsufuji, S. Iguchi, Y. Taguchi, H. Takagi, and Y. Tokura, Phys. Rev. B **70**, 100401(R) (2004).
- [34] M. L. Sanjuan, C. Guglieri, S. Dáz-Moreno, G. Aquilanti, A. F. Fuentes, L. Olivi, and J. Chaboy, Phys. Rev. B **84**, 104207 (2011).
- [35] C. L. Tracy, J. Shamblin, S. Park, F. Zhang, C. Trautmann, M. Lang, and R. C. Ewing, Phys. Rev. B **94**, 064102 (2016).
- [36] T. S. Sreena, P. Prabhakar Rao, T. L. Francis, A. K. V. Raj and P. S. Babu, Dalton Trans. **44**, 8718 (2015)
- [37] E. Granado, P. G. Pagliuso, J. A. Sanjurjo, M. A. Subramanian, S.-W Cheong, S. B. Oseroff and C. Rettori, Phys. Rev. B **60**, 6513 (1999).
- [38] B. Mihailova, S. Stoyanov, V. Gaydarov, M. Gospadinov, and L. Konstantinov, Solid State Commun. **103**, 623 (1997).
- [39] S. Saha, S. Singh, B. Dkhil, S. Dhar, R. Suryanarayanan, G. Dhahenne, A. Revcolevschi, and A. K. Sood, Phys. Rev. B **78**, 214102 (2008).
- [40] J. Vermette, S. Jandl and M. M. Gospodinov, J. Phys.: Condens. Matter **20**, 425219 (2008).
- [41] E. Granado, A. Garcia, J. A. Sanjurjo, C. Rettori, and I. Torriani, Phys. Rev. B **60**, 11879 (1999).
- [42] M. K. Crawford, M. A. Subramanian, and R. L. Harlow, Phys. Rev. B **49**, 9198 (1994).
- [43] I. N. Bhatti, R. Rawat, A. Banerjee and A. K. Pramanik, J. Phys.: Condens. Matter **27** 016005 (2014).
- [44] I. N. Bhatti and A. K. Pramanik, J. Magn. Magn. Mater **422** 141 (2017).